Water Science & Technology

IWA PUBLISHING

Water Science & Technology Vol 88 No 6, 1417 doi: 10.2166/wst.2023.268

Synthesis of PES membranes modified with polyurethane–paraffin wax nanocapsules and performance of bovine serum albumin and humic acid rejection

Buse Sert[a], Gül Kaya[a], Yasin Ozay[b], Aya Alterkaoui[c], Kasım Ocakoglu[a] and Nadir Dizge[c,*]

[a] Department of Engineering Fundamental Sciences, Faculty of Engineering, Tarsus University, Tarsus 33400, Turkey
[b] Department of Environmental Protection Technologies, Tarsus University, Mersin 33400, Turkey
[c] Department of Environmental Engineering, Mersin University, Mersin 33343, Turkey
*Corresponding author. E-mail: nadirdizge@gmail.com

ABSTRACT

Membrane fouling is a serious handicap of membrane-based separation, as it reduces permeation flux and hence increases operational and maintenance expenses. Polyurethane–paraffin wax (PU/PW) nanocapsules were integrated into the polyethersulfone membrane to manufacture a composite membrane with higher antifouling and permeability performance against humic acid (HA) and bovine serum albumin (BSA) foulants. All manufactured membranes were characterized by scanning electron microscopy (SEM), scanning electron microscopy-energy dispersive spectrometry (SEM-EDS), and contact angle. The contact angle of the pristine polyethersulfone (PES) membrane was measured 73.40 ± 1.32. With the embedding of nanocapsules, the contact angle decreased to 64.55 ± 1.23 for PES/PU/PW 2.0 wt%, and the pure water flux of all composite membranes increased when compared to pristine PES. The pristine PES membrane also has shown the lowest steady-state fluxes at 45.84 and 46.59 L/m^{2}h for BSA and HA, respectively. With the increase of PU/PW nanocapsule ratio from 0.5 to 1.0 wt%, steady-state fluxes increased from 51.96 to 71.61 and from 67.87 to 98.73 L/m^{2}h, respectively, for BSA and HA. The results depicted that BSA and HA rejection efficiencies of PU/PW nanocapsules blended PES membranes increased when compared to pristine PES membranes.

Key words: composite PES membrane, humic acid separation, polyurethane–paraffin wax nanocapsules, protein separation

HIGHLIGHTS

- Polyurethane–paraffin wax nanocapsules were integrated into the polyethersulfone membrane.
- The contact angle decreased from 73.40 ± 1.32° to 64.55 ± 1.23° for PES/PU/PW 2.0 wt%.
- BSA and HA rejection efficiencies of the PES/PU/PW 1.0% membrane increased from 93.95 to 100% and 98.78 to 100%, respectively.

GRAPHICAL ABSTRACT

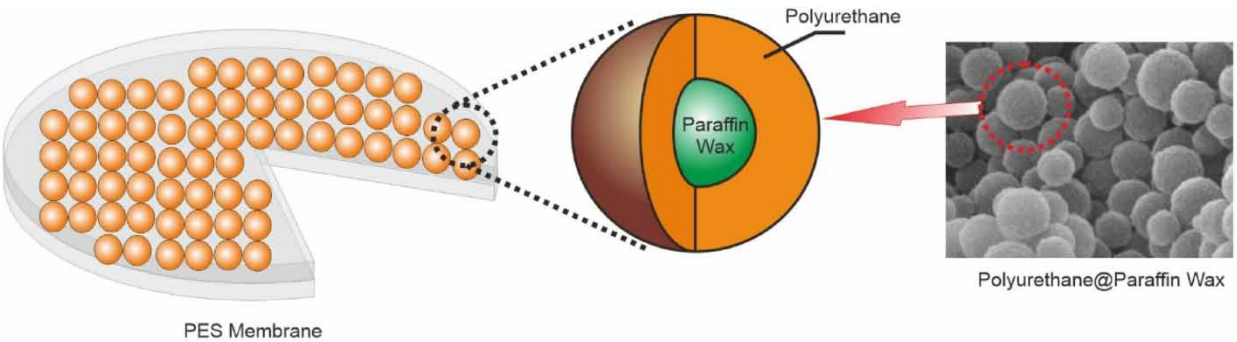

1. INTRODUCTION

Water scarcity and pollution have become a worldwide concern as a result of growing urbanization, industry, and technological advancements, posing a threat to the entire ecosystem and harming human health (Arenas-Sánchez *et al.* 2016).

Membrane technology is still the most effective treatment and water recovery system, with the best prospects in wastewater applications, as compared to other physical, chemical, physicochemical, or biological treatment systems (Nasir *et al.* 2022). Sadly, the most significant disadvantage of membrane-based separation is membrane fouling, which decreases the permeation flux and hence raises operational and maintenance costs (Barambu *et al.* 2021; Li *et al.* 2021; Qiu *et al.* 2022). Therefore, the membrane surface needs to be modified in various ways to prevent the fouling mechanism.

Phase change materials (PCMs) with a crystalline structure are organic or inorganic compounds that can absorb and store energy as latent heat and release energy depending on temperature differences during the phase change process, melting and freezing, evaporation and condensation, or changes in the crystal structure (Jin *et al.* 2008; Atinafu *et al.* 2020; Yang *et al.* 2021). In addition to the chemical properties of latent heat storage PCMs such as non-toxic, non-corrosive, non-flammable, non-explosive, and chemically stable for a long time, physical (high density, low vapor pressure, and small volume changes at phase transitions), thermal (high thermal conductivity, high latent heat, and high specific heat), and kinetic properties (absence of subcooling and having a suitable crystallization rate) also draw attention (Shchukina *et al.* 2018; Vadhera *et al.* 2018; Rodríguez-Cumplido *et al.* 2019). Moreover, the low cost and abundance of PCMs are important factors in their applicability in a variety of fields (Vadhera *et al.* 2018). PCMs have the potential to be used in application areas like energy (Gupta *et al.* 2020; Faraj *et al.* 2021; Zhi *et al.* 2022), environment (Lamnatou *et al.* 2018; Dibene *et al.* 2020; Roy *et al.* 2021), textiles (Aitali *et al.* 2016; Lu *et al.* 2019; Saraç *et al.* 2019; AitAli *et al.* 2023), and medicine (Li *et al.* 2015, 2019) due to their phase transition temperatures and characteristics. PCMs are classified as organic, inorganic, or eutectic. Among them, paraffin, which is one of the organic PCMs, stands out with its important properties such as non-corrosive, chemically inert, low vapor pressure during the melting phase, and non-toxicity (Magendran *et al.* 2019; Ghasemi *et al.* 2022). However, paraffin's limited heat conductivity, absence of a stable melting point, and flammability limit their application possibilities. As a result, various solutions have been created, especially to solve the problem of low thermal conductivity, and the most common of these is the method of keeping paraffin in polymeric mesh such as polyurethane and polyethylene (Vasu *et al.* 2019; Nikpourian *et al.* 2020). Microencapsulation and nanoencapsulation methods applied for this purpose are used to eliminate the disadvantages of paraffin. PCMs coated by microencapsulation or nanoencapsulation methods are small core-shell particles coated with inorganic or polymer materials. The nanoencapsulation approach improves the microencapsulation method by reducing the surface-to-volume ratio by shrinking the capsule to nanoscale size. Thus, the heat transfer rate increases with the nano-encapsulated PCMs obtained from Zhang & Yuan (2020), Peng *et al.* (2021), and Cao *et al.* (2022). Abdeali *et al.* employed a polymerization procedure to generate nano-encapsulated paraffin wax core/polyurethane shell (PW/PU) and determined that the sonication time and reaction temperature had a good effect on thermal performance by creating narrow particle size distribution, according to the findings (Abdeali *et al.* 2021). The incorporation of PCMs into the UF membrane matrix can increase its thermal stability and improve its resistance to temperature variations. This can be particularly useful in applications where the temperature of the feed solution needs to be maintained within a narrow range, as the PCM can help to absorb or release thermal energy and prevent fluctuations in the feed solution temperature (Wang *et al.* 2014). In addition, the use of PCM-modified UF membranes can enhance the separation performance of the membrane. PCMs can reduce fouling and enhance the permeate flux by reducing the adhesion of foulants to the membrane surface, resulting in better membrane cleaning and longer membrane lifespan (Fakhry *et al.* 2022).

In this study, nano-encapsulated paraffin wax core/thermoplastic elastomer polyurethane shell (PW/PU) was synthesized by the mini-emulsion polymerization method. The synthesized PW/PU nanocapsules were characterized and validated by scanning electron microscopy (SEM), thermogravimetric analysis (TGA), differential scanning calorimetry (DSC), and Fourier-transform infrared spectroscopy (FTIR) analyses. Confirmed by characterization methods, polyurethane–paraffin wax (PU/PW) nanocapsules were integrated into the polyethersulfone (PES) membrane to form a composite membrane with higher antifouling and permeability performance against humic acid (HA) and bovine serum albumin (BSA) foulants. To the best of our knowledge, no studies on PES membranes modified with PU/PW nanocapsules have been reported in the literature.

2. MATERIALS AND METHODS

2.1. Materials

Isophorone diisocyanate, polyethylene glycol (PEG6000), cyclohexanone, paraffin wax, 1-dodecanol, glycerol, sodium dodecyl sulfate (≥99.0%), polycaprolactone (MW: 10,000), and HA were purchased from Sigma Aldrich and used without

additional purification. BASF Company (Germany) provided polyethersulfone (PES, Ultrason E6020P, MW: 58,000 g/mol). Dimethyl sulfoxide (DMSO) and bovine serum albumin (BSA, MW: 66,000 g/mol) were supplied from Merck Company (Germany). All chemicals were analytical grade, and distilled water was obtained using a Millipore Direct-Q3UV purification system with two stages.

2.2. Synthesis of PU/PW nanocapsules

PU/PW nanocapsules were synthesized in accordance with the literature (Abdeali *et al.* 2021). In a typical synthesis of the PU/PW nanocapsules, 2 g of sodium dodecyl sulfate (0.006 mol) is first dissolved in 10 mL of deionized water under inert gas, and the organic phase containing 0.6 g of isophorone diisocyanate (IPDI), 0.1 g of paraffin wax, and 0.14 g of cyclohexanone (0.0014 mol) are mixed thoroughly in a separate beaker. Subsequently, both phases are brought together in an inert atmosphere and allowed to mix at 80 °C. The mixture was ultrasonicated for 15 min and 0.12 g of PEG6000 was added to the medium and mixed for 1 h. About 0.16 g of polycaprolactone and 0.16 g of glycerol were added to the medium, and the mixing was continued for another 3 h. After adding 0.3 g of 1-dodecanol (0.0016 mol) to the medium, PU/PW dispersion was filtered and washed through centrifugation (10,000 rpm, 15 min, several times) using hot deionized water and cyclohexanone. Finally, obtained PU/PW nanocapsules were freeze-dried in a vacuum. The zeta potential of PU/PW nanocapsules was determined using a zeta sizer (Malvern Zetasizer equipped with MPT-2 Titrator, Nano ZS). The samples were prepared using deionized water as a 0.1% solution, and the pH of the solution was adjusted to 7.0.

2.3. Preparation of neat and PU/PW nanocapsules blended PES membranes

The phase inversion method was used to manufacture the neat and PU/PW nanocapsules blended membranes. Before using the PES beads, they were dried at 80 °C in an oven for 2 h. To manufacture functionalized membranes, first, the different ratios of PU/PW nanocapsules (0.5, 1.0, and 2.0 wt%) were added to DMSO solvent and dispersed for 15 min by using an ultrasonication bath, and PES beads were then added to this solution. The prepared solution was rapidly shaken at 60 °C for 6 h and after that at room temperature overnight then ultrasonicated for 20 min again to obtain a clear homogeneous solution and remove air bubbles from the casting solutions. When all bubbles were removed, casting solutions of PU/PW nanocapsules were spread on a glass plate with a casting knife gap setting of 200 μm at a speed of 100 mm/s. The glass plates were subsequently immersed in a deionized water bath to achieve polymer sedimentation. The membranes were withdrawn from the water bath and kept in fresh deionized water for at least 1 day after manufacture to ensure complete phase inversion. The casting solution's composition is shown in Table 1. Before the experiments, all membranes were operated at 5 bar with deionized water.

2.4. Characterization of pristine and composite membranes

The surface morphology of the manufactured pristine PES membrane and PU/PW nanocapsules blended PES membranes were characterized by scanning electron microscopy (SEM, Gemini Zeiss Supra 55). The membranes were coated with a gold layer after drying at room temperature. The SEM images were taken using a 20.0 kV acceleration voltage. The contact angle of all the manufactured membranes is measured to determine their surface hydrophilicity. A dead-end flat sheet membrane module with a filtration area of 14.6 cm^2 was used to test the filtration performance of the manufactured membranes at a temperature of 25 $\pm$ 1 °C and an operating pressure of 1 bar.

Table 1 | The manufactured membranes' casting solution composition (composition in wt%)

Membrane sample	PES	DMSO	PU/PW
Pristine PES	14	86.0	0.00
PES/PU/PW 0.5 wt%	14	85.5	0.50
PES/PU/PW 1.0 wt%	14	85.0	1.00
PES/PU/PW 2.0 wt%	14	84.0	2.00

The permeation flux (J) was calculated by using the following equation after collecting the filtered water in the prescribed intervals (Ganjali *et al.* 2021).

$$J = \frac{V}{A \times \Delta t} \tag{1}$$

where J is the permeate flux (L/m^{2}h); V is the volume of permeate pure water (L), A is the effective area of the membrane (m^2), and Δt is the filtration time (h).

The overall porosity (ε) was calculated by the gravimetric method. Further details on the porosity calculation can be found elsewhere (Ocakoglu *et al.* 2021). The overall porosity (ε) of the prepared membranes was determined using Equation (2) based on the gravimetric method.

$$\varepsilon = \frac{W_w - W_d}{\rho_w \times A \times \lambda} \times 100 \tag{2}$$

where W_w is the weight of the wet membrane (g); W_d is the weight of the dry membrane (g); ρ_w is the density of pure water at room temperature (0.998 g/cm^3); A is the effective area of the membrane (cm^2), and λ is the membrane thickness (cm).

Furthermore, the mean pore radius (r_p) on the basis of the pure water flux and porosity data was calculated by the Guerout–Elford–Ferry equation.

$$r_p = \sqrt{\frac{(2.9 - 1.75\varepsilon)8\eta\lambda Q}{\varepsilon \times A \times \Delta P}} \tag{3}$$

where r_p is the mean pore radius (nm); η is water viscosity (8.9×10^{-4} Pa s); λ is the membrane thickness (m); Q is the volume of the permeate water per unit time (m^3/s); and ΔP is the operating pressure (0.1 MPa).

2.5. Protein and HA rejection experiments of the membranes

The dead-end filtration system was filled separately with 100 mg/L of BSA solution and 50 mg/L of HA solution to test the efficiency of the manufactured membranes. To prevent the denaturation of protein, BSA solution was prepared in phosphate buffer solution (PBS, 50 mM, pH 7.4 $\pm$ 0.1). Both solutions were filtrated at 1 bar for 120 min. The Lowry method (Lowry *et al.* 1951) was used to determine the protein concentration of the feed (C_f) and permeate (C_p). The HA concentration in the solution is represented by total organic carbon (TOC) content, which was measured by using a TOC analyzer (Elementar, Vario TOC Cube). The desorption experiments for BSA and HA, which were adsorbed onto the membrane surface, were conducted by separately filtering them for 150 min at prepared concentrations. Afterward, the membranes were placed in pure water and agitated using an orbital shaker to measure the time-dependent amounts of BSA and HA pollutants on their surfaces that passed into the pure water.

3. RESULTS AND DISCUSSION

3.1. Characterization of PU/PW nanocapsules

An SEM image of the synthesized material is shown in Figure 1. An SEM image indicated that PU/PW nanocapsules with spherical, nanoscale core–PU shell structures were synthesized. The particle diameters of the synthesized PU/PW nanocapsule are 110–220 nm.

FTIR analysis of the synthesized material is shown in Figure 2. According to the results of the FTIR analysis, the peaks of 3,337 and 1,554 cm^{-1} show N–H stretching vibration and N–H bending vibrations, and these vibrations show urethane bond formation. The peaks of 2,906, 1,402, and 1,221 cm^{-1} are the CH stretching vibrations of the CH_3 group and the CH_2 group for long chain bonds, respectively, and these peaks belong to the PW core spectra. In addition, PU/PW nanocapsule spectra show the complete reaction of IPDI during the 2,255 cm^{-1} peak PU/PW nanocapsule synthesis (Abdeali *et al.* 2021).

TGA and DSC analyses can provide valuable information about the thermal stability and phase behavior of the composite materials. TGA analysis of the synthesized material is shown in Figure 3. According to the TGA analysis results shown in Figure 3(a), a decrease in the PU/PW weight occurs with an increase in temperature. A one-step decomposition occurs in the PU/PW nanocapsule structure depending on the temperature.

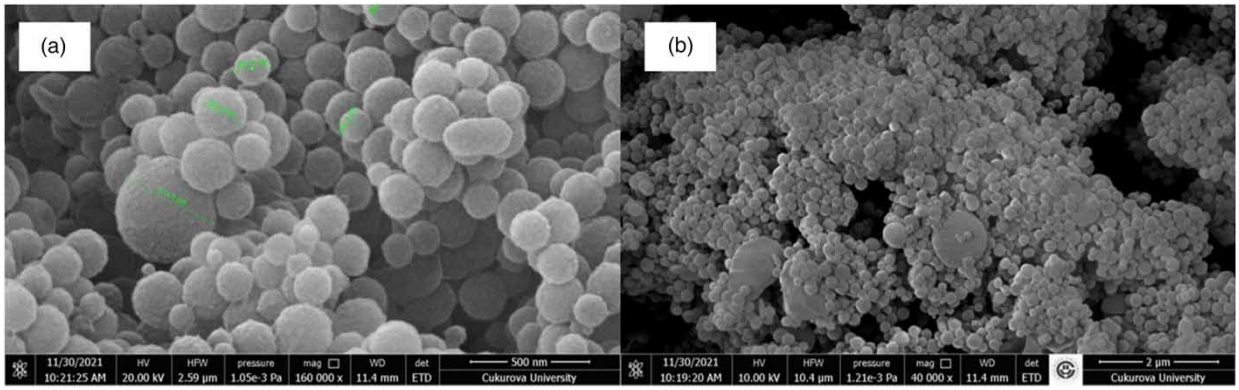

Figure 1 | The representative SEM images in different magnifications of the prepared PU/PW nanocapsule.

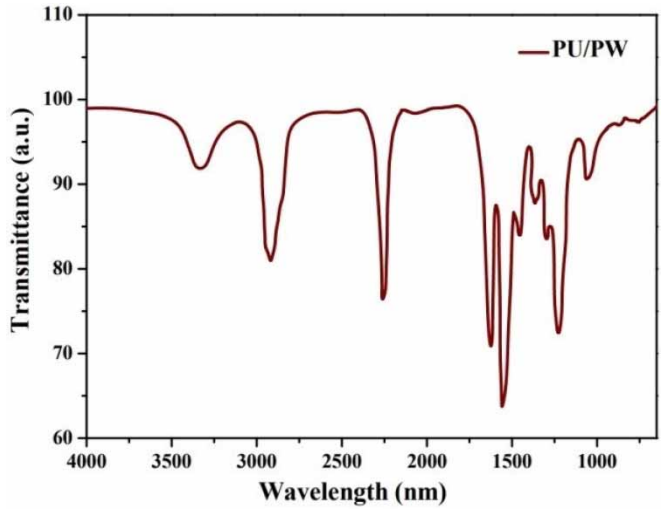

Figure 2 | FTIR analysis of the synthesized PU/PW nanocapsule. Please refer to the online version of this paper to see this figure in colour: https://dx.doi.org/10.2166/wst.2023.268.

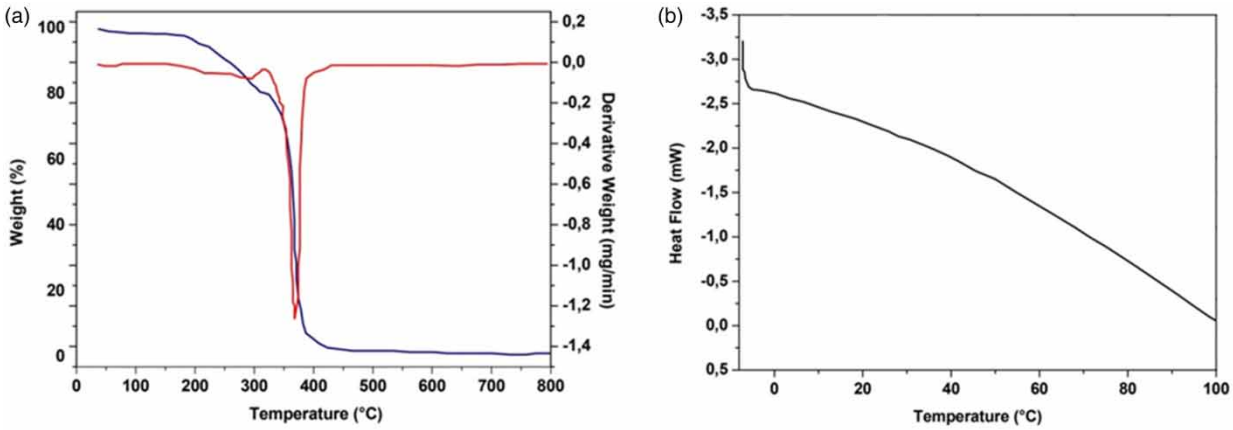

Figure 3 | (a) TGA and (b) DSC analysis of the synthesized PU/PW nanocapsule.

According to the results of the TGA analysis, approximately 92% mass loss occurred, and from the DTG curve (red curve) given in the TGA analysis, it is seen that the maximum temperature value at which degradation occurs is 367.8 °C. This temperature value obtained from the DTG curve shows the highest material loss at 367.8 °C. DSC analysis of the synthesized material is shown in Figure 3(b). The endothermic peak at 49.9 °C is seen in the DSC analysis graph, and this peak belongs to the PU/PW nanocapsules. The use of PU/PW nanocapsules provided delayed temperature increases.

3.2. Characterization of PU/PW nanocapsules blended PES membranes

The surface SEM micrographs of the manufactured pristine and PU/PW nanocapsules blended PES membranes are shown in Figure 4. On the pristine membrane, there was a smooth surface. The PU/PW nanocapsules, which are spherical, have coated the surface of the PES membranes in a very smooth pattern, as shown by SEM micrographs. As the concentration increases from 0.5 to 2.0%, the amount of PU/PW capsules on the surface increases.

The surface SEM micrographs of PES PU/PW 2.0 wt% membranes after 2 h of filtration of BSA and HA are shown in Figure 5. It is clearly visible that the cake layer formed during the filtration process covers the membrane surface for both pollutants. The molecular weight of HA is relatively higher compared to BSA, which has a molecular weight of 66.5 kDa, and as observed, the fouling occurring on the membrane surface is, therefore, more pronounced.

The energy dispersive spectrometry (EDS) mapping of pristine and PU/PW nanocapsules blended PES membrane depicted that the elementary components were composed of C, O, and S (Table 2). It can be seen the increase in the C ratio and the decrease in the O and S ratio indicate that the PU/PW is successfully involved in the membrane structure.

The porosity and mean pore size of the membranes are presented in Table 3. The results showed that the porosity of the membranes decreased from 62.5 $\pm$ 1.1 to 55.5 $\pm$ 1.2% after blended of PU/PW nanocapsules. Moreover, the mean pore radius decreased from 24.8 $\pm$ 0.35 to 17.7 $\pm$ 0.19 nm.

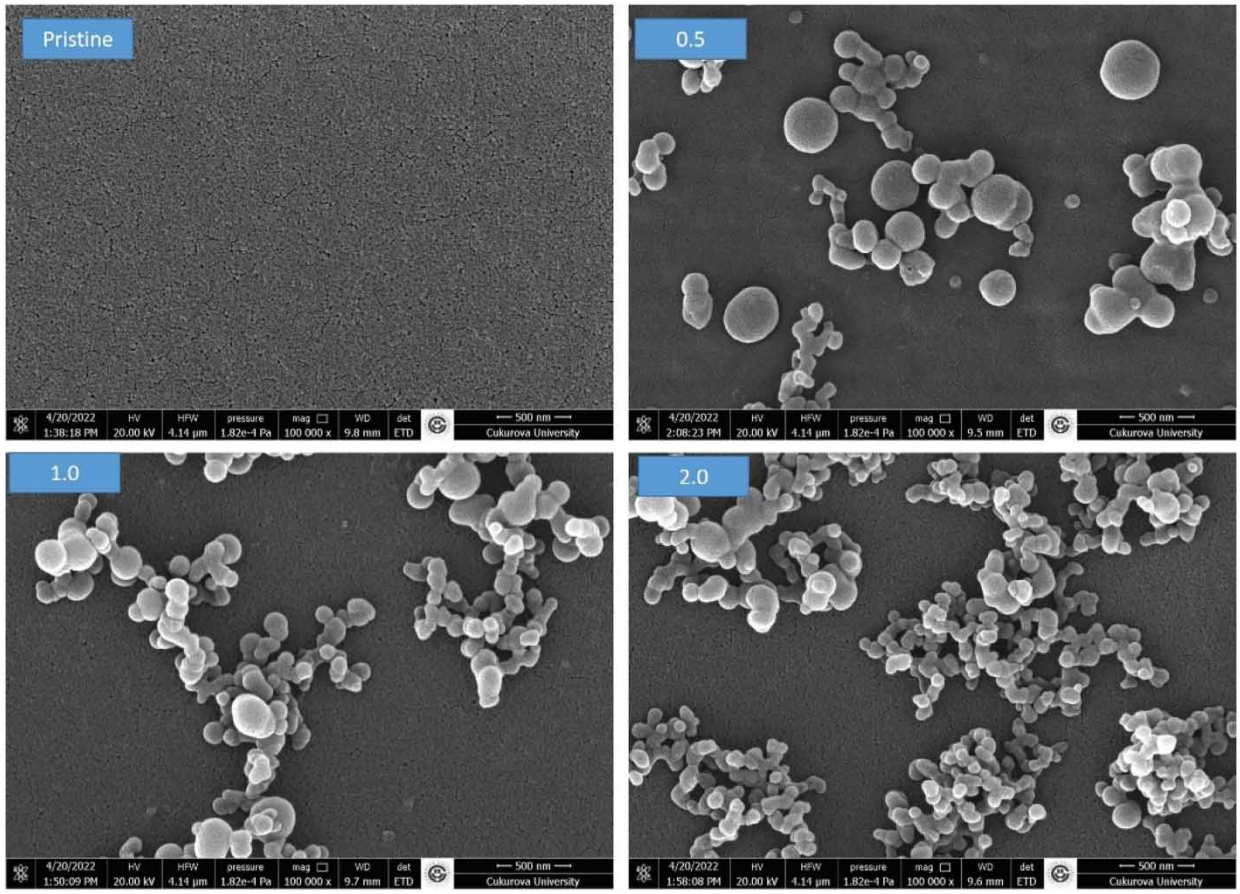

Figure 4 | SEM images of PES membranes blended with different ratios of PU/PW nanocapsules (pristine and PU/PW compositions in wt%).

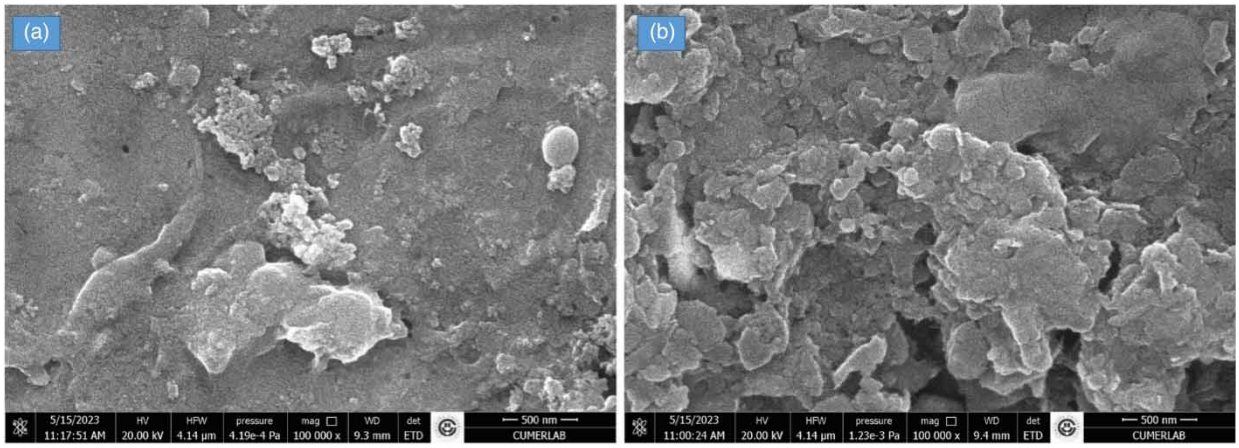

Figure 5 | SEM images of PES/PU/PW 2.0 wt% membranes after (a) BSA and (b) HA filtration.

Table 2 | EDS of the pristine and PU/PW nanocapsules blended PES membranes

Percentages of the elements (wt%)	Pristine membrane	PES/PU/PW 0.5 wt%	PES/PU/PW 1.0 wt%	PES/PU/PW 2.0 wt%
C	54.93	60.0	62.49	62.61
O	20.36	16.99	15.5	17.58
S	24.71	23.01	22.02	19.81

Table 3 | Porosity and mean pore size of the membranes

Membrane type	Porosity (%)	Mean pore radius (nm)
Pristine PES	62.5 $\pm$ 1.1	24.8 $\pm$ 0.35
PES/PU/PW 0.5 wt%	60.8 $\pm$ 1.3	22.1 $\pm$ 0.29
PES/PU/PW 1.0 wt%	57.6 $\pm$ 1.5	19.8 $\pm$ 0.32
PES/PU/PW 2.0 wt%	55.5 $\pm$ 1.2	17.7 $\pm$ 0.19

For pristine PES and PU/PW nanocapsules blended PES membranes, the variation of deionized water permeability coefficient (J_p) against transmembrane pressure (TMP) was investigated (Figure 6(a)). According to the Darcy law, there is a straight linear relationship between pressure operation and permeate flux. The pure water permeate of PU/PW nanocapsules blended PES membranes showed better performance against pristine PES membranes, but a decrease was observed with an increasing PU/PW ratio. It is known that the contact angle is related to the membrane hydrophilicity and when compared to hydrophobic membranes, hydrophilic membranes have a lower flux reduction (Figure 6(b)) (Celik *et al.* 2011). The contact angle of the pristine PES membrane has measured 73.40 $\pm$ 1.32. With the increase of nanocapsule ratio, the contact angle decreased from 67.23 $\pm$ 1.82 to 64.55 $\pm$ 1.23 for PU/PW blended membranes. Despite the increase in hydrophilicity, the modified membranes showed a decrease in the permeance of pure water. This could be attributed to the blockage of membrane pores caused by the nanocapsules, which is supported by the fact that the pore size distribution of all modified membranes was narrower than that of the pristine ones (Zhao *et al.* 2013; Kasemset *et al.* 2017).

3.3. BSA and HA flux performance of PU/PW nanocapsules blended PES membranes

The ability of the membrane to filter solutions, also known as flux or permeability, is a key metric for its performance. Another essential feature is the membrane's ability to remove components or particles from the solution, which is referred to as solute rejection (Field & Wu 2022). BSA and HA fluxes are given in Figure 7(a) and 7(b). The pristine PES membrane

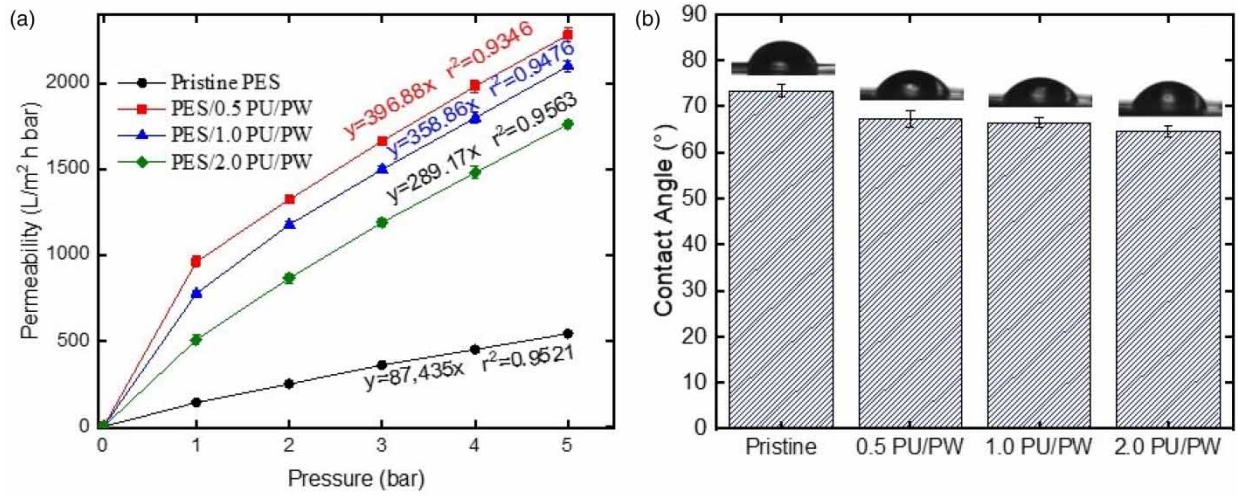

Figure 6 | (a) Variation of permeability coefficient (J_p) of deionized water against TMP and (b) contact angle.

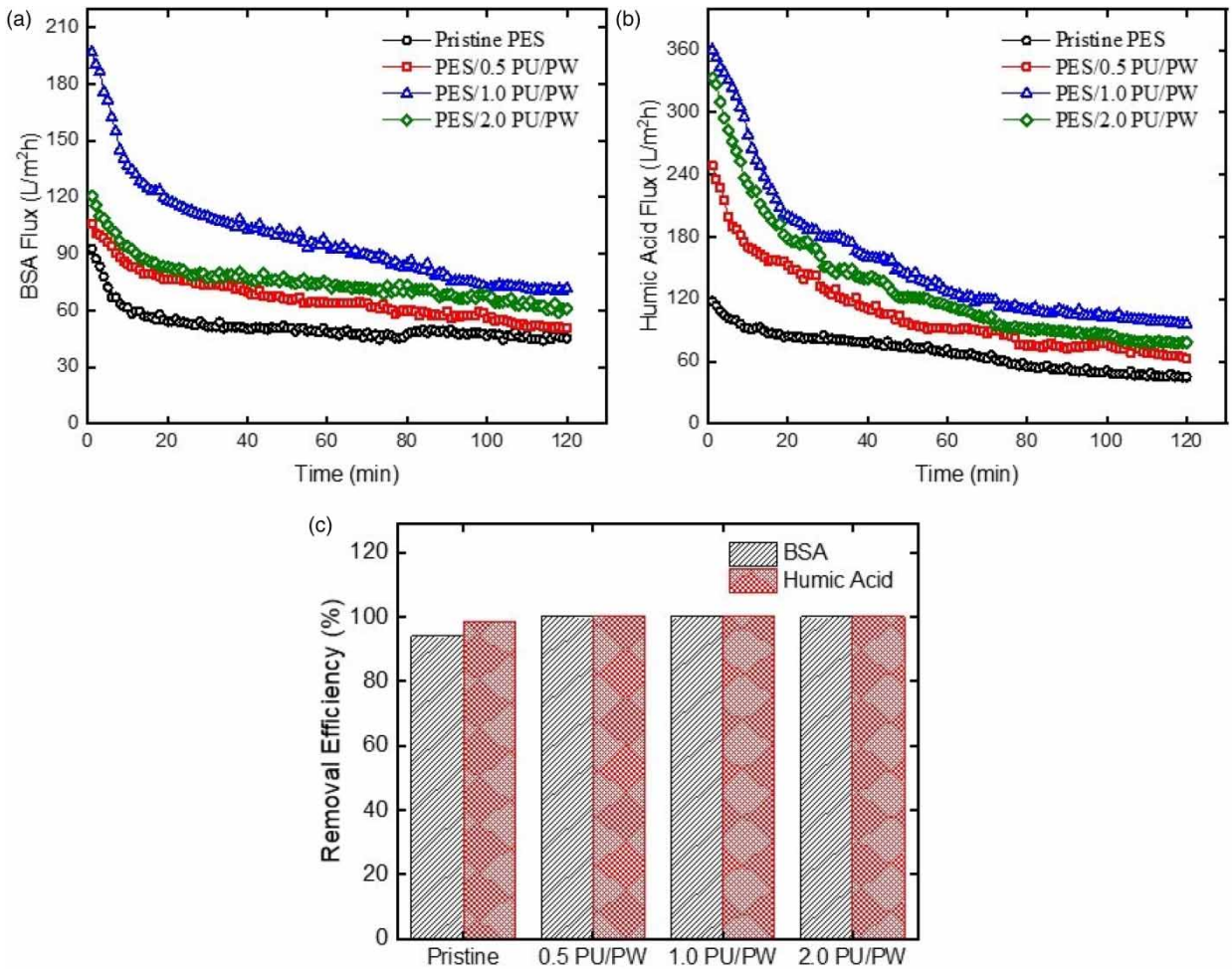

Figure 7 | (a) BSA, (b) humic acid flux and (c) removal efficiencies of pristine and PU/PW nanocapsules blended PES membranes.

has shown the lowest steady-state fluxes at 45.84 and 46.59 L/m^{2}h for BSA and HA. With the increase of PU/PW nanocapsule ratio from 0.5 to 1.0 wt%, steady-state fluxes increased from 51.96 to 71.61 and from 67.87 to 98.73 L/m^{2}h, respectively, for BSA and HA. However, for the PES/PU/PW 2.0 wt% membrane, it was observed that the steady-state flux did not increase but slightly decreased, compared to PES/PU/PW 1.0%. The agglomeration of PU/PW nanocapsules in the structure of composite membranes and the balking of the pores, resulting in smaller pore-sized membranes, could explain this decrease. The manufactured membranes' capacity to reject BSA and HA was also investigated (Figure 7(c)). Due to the PU/PW nanocapsules present in the membrane matrix rendering the membrane surface hydrophilic, composite membranes are expected to attract water molecules more effectively during filtration, resulting in higher permeability (Wang *et al.* 2022). On the other hand, it was observed that the zeta potential of the PU/PW nanocapsules in pure water was negatively charged (−81.46 mV) at neutral pH. When the surface of PES membranes is uncharged, it is expected that the inclusion of PU/PW nanocapsules into the membrane matrix would result in a negative surface charge. It is known from previous studies in the literature that BSA and HA also have a negative charge under neutral pH conditions (Xu *et al.* 2003; Klučáková 2018). The BSA and HA rejection efficiencies of PU/PW nanocapsule blended PES membranes also increased significantly compared to pristine PES membranes, with BSA rejection increasing from 93.95 to 100% and HA rejection increasing from 98.78 to 100%. It can be inferred that having a negative surface charge on the membrane, while pollutants like BSA and HA are negatively charged as well, improves both the removal efficiency of these pollutants and the flux performance. Therefore, it can be concluded that the increased hydrophilicity contributed to the improved BSA and HA rejection. The results obtained after the desorption of BSA and HA pollutants adsorbed on the membrane surface are presented in Figure 7(d). The total desorption amounts for BSA and HA were 22.27 and 8.42 μg/cm^2, respectively.

4. CONCLUSION

In this study, nano-encapsulated paraffin wax core/thermoplastic elastomer polyurethane shell (PW/PU) was synthesized by the mini-emulsion polymerization method and then it is used for manufacturing PU/PW nanocapsules blended PES membranes by the phase inversion method. PU/PW nanocapsules were characterized by SEM, TGA, DSC, and FTIR analyses. The use of PU/PW nanocapsules provided delayed temperature increases, which are confirmed by DSC. All membranes were characterized by SEM, SEM-EDS, and contact angle. After the PU/PW nanocapsules were dispersed into the PES membrane, the composite membranes' hydrophilicity increased. BSA and HA are used to test the antifouling and permeability performance of manufactured membranes. The pure water, BSA, and HA fluxes of the composite membranes increased compared to the pristine PES membrane. PU/PW nanocapsules blended PES membranes can be used to decrease membrane fouling.

AUTHORS' CONTRIBUTIONS

B.S., G.K., Y.O. and A.A. performed methodology and data curation. K.O. and N.D. conceptualized, investigated, and wrote the original draft and did formal analysis and reviewed and edited the manuscript.

FUNDING

This research received no specific grant from any funding agency in the public, commercial, or not-for-profit sectors.

DATA AVAILABILITY STATEMENT

All relevant data are included in the paper or its Supplementary Information.

CONFLICT OF INTEREST

The authors declare there is no conflict.

REFERENCES

Abdeali, G., Abdollahi, M. & Bahramian, A. R. 2021 Synthesis and characterization of paraffin wax nanocapsules with polyurethane shell (PU/PW); the droplet size distribution: a key factor for thermal performance. *Renewable Energy* **163**, 720–731.

Aitali, S., Kebiche-Senhadji, O. & Benamor, M. 2016 Performance of an acidic extractant (D2EHPA) incorporated in IM used for extraction and separation of Methylene Blue and Rhodamin B. *Membrane Water Treatment* **7** (6), 521–537.

AitAli, S., Ziani, S., Yahiaoui, I., Brahmi, A., Boudrahem, F. & Aissani-Benissad, F. 2023 Application of central composite design and response surface methodology for the study of extraction of gentian violet dye in aqueous solution by polystyrene membrane modified with oleic acid. *Environmental Progress & Sustainable Energy* **e14200**, 1–12.

Arenas-Sánchez, A., Rico, A. & Vighi, M. 2016 Effects of water scarcity and chemical pollution in aquatic ecosystems: state of the art. *Science of the Total Environment* **572**, 390–403.

Atinafu, D. G., Ok, Y. S., Kua, H. W. & Kim, S. 2020 Thermal properties of composite organic phase change materials (PCMs): a critical review on their engineering chemistry. *Applied Thermal Engineering* **181**, 115960.

Barambu, N. U., Bilad, M. R., Laziz, A. M., Nordin, N. A. H. M., Bustam, M. A., Shamsuddin, N. & Khan, A. L. 2021 A wavy flow channel system for membrane fouling control in oil/water emulsion filtration. *Journal of Water Process Engineering* **44**, 102340.

Cao, Y., Farouk, N., Ayed, H., Aly, A. A., Jarad, F., Dahari, M., Wae-hayee, M. & Saleh, B. 2022 Heat transfer improvement between a pair of heater and cooler inside an energy storage by using nano-encapsulated phase change material/water: a numerical modeling. *Case Studies in Thermal Engineering* **30**, 101770.

Celik, E., Park, H., Choi, H. & Choi, H. 2011 Carbon nanotube blended polyethersulfone membranes for fouling control in water treatment. *Water Research* **45** (1), 274–282.

Dibene, K., Yahiaoui, I., Yahia Cherif, L., Aitali, S., Amrane, A. & Aissani-Benissad, F. 2020 Paracetamol degradation by photo-activated peroxydisulfate process (UV/PDS): kinetic study and optimization using central composite design. *Water Science and Technology* **82** (7), 1404–1415.

Fakhry, H., El-Sonbati, M., Omar, B., El-Henawy, R., Zhang, Y. & El-Kady, M. 2022 Novel fabricated low-cost hybrid polyacrylonitrile/polyvinylpyrrolidone coated polyurethane foam (PAN/PVP@PUF) membrane for the decolorization of cationic and anionic dyes. *Journal of Environmental Management* **315**, 115128.

Faraj, K., Khaled, M., Faraj, J., Hachem, F. & Castelain, C. 2021 A review on phase change materials for thermal energy storage in buildings: heating and hybrid applications. *Journal of Energy Storage* **33**, 101913.

Field, R. W. & Wu, J. J. 2022 Permeate flux in ultrafiltration processes – understandings and misunderstandings. *Membranes* **12** (2), 1–18.

Ganjali, M. R., Al-Naqshabandi, M. A., Larijani, B., Badiei, A., Vatanpour, V., Rajabi, H. R., Rezania, H., Paziresh, S., Mahmodi, G., Kim, S. J. & Saeb, M. R. 2021 Improvement of dye and protein filtration efficiency using modified PES membrane with 2-mercaptoethanol capped zinc sulfide quantum dots. *Chemical Engineering Research and Design* **168**, 109–121.

Ghasemi, K., Tasnim, S. & Mahmud, S. 2022 PCM, nano/microencapsulation and slurries: a review of fundamentals, categories, fabrication, numerical models and applications. *Sustainable Energy Technologies and Assessments* **52**, 102084.

Gupta, B., Bhalavi, J., Sharma, S. & Bisen, A. 2020 Phase change materials in solar energy applications: a review. *Materials Today: Proceedings* **46**, 5550–5554.

Jin, Z., Wang, Y., Liu, J. & Yang, Z. 2008 Synthesis and properties of paraffin capsules as phase change materials. *Polymer* **49** (12), 2903–2910.

Kasemset, S., Wang, L., He, Z., Miller, D. J., Kirschner, A., Freeman, B. D. & Sharma, M. M. 2017 Influence of polydopamine deposition conditions on hydraulic permeability, sieving coefficients, pore size and pore size distribution for a polysulfone ultrafiltration membrane. *Journal of Membrane Science* **522**, 100–115.

Klučáková, M. 2018 Size and charge evaluation of standard humic and fulvic acids as crucial factors to determine their environmental behavior and impact. *Frontiers in Chemistry* **6**, 235.

Lamnatou, C., Motte, F., Notton, G., Chemisana, D. & Cristofari, C. 2018 Building-integrated solar thermal system with/without phase change material: life cycle assessment based on ReCiPe, USEtox and ecological footprint. *Journal of Cleaner Production* **193**, 672–683.

Li, J., Hu, Y., Hou, Y., Shen, X., Xu, G., Dai, L., Zhou, J., Liu, Y. & Cai, K. 2015 Phase-change material filled hollow magnetic nanoparticles for cancer therapy and dual modal bioimaging. *Nanoscale* **7** (19), 9004–9012.

Li, Q., Sun, L., Hou, M., Chen, Q., Yang, R., Zhang, L., Xu, Z., Kang, Y. & Xue, P. 2019 Phase-change material packaged within hollow copper sulfide nanoparticles carrying doxorubicin and chlorine 6 for fluorescence-guided trimodal therapy of cancer. *ACS Applied Materials and Interfaces* **11** (1), 417–429.

Li, P., Yang, C., Sun, F. & Li, X. Y. 2021 Fabrication of conductive ceramic membranes for electrically assisted fouling control during membrane filtration for wastewater treatment. *Chemosphere* **280**, 130794.

Lowry, O. H., Rosebrough, N. J., Farr, A. L. & Randall, R. J. 1951 Protein measurement with the Folin phenol reagent. *The Journal of Biological Chemistry* **193** (1), 265–275.

Lu, Y., Xiao, X., Fu, J., Huan, C., Qi, S., Zhan, Y., Zhu, Y. & Xu, G. 2019 Novel smart textile with phase change materials encapsulated core-sheath structure fabricated by coaxial electrospinning. *Chemical Engineering Journal* **355**, 532–539.

Magendran, S. S., Khan, F. S. A., Mubarak, N. M., Vaka, M., Walvekar, R., Khalid, M., Abdullah, E. C., Nizamuddin, S. & Karri, R. R. 2019 Synthesis of organic phase change materials (PCM) for energy storage applications: a review. *Nano-Structures and Nano-Objects* **20**, 100399.

Nasir, A. M., Adam, M. R., Mohamad Kamal, S. N. E. A., Jaafar, J., Othman, M. H. D., Ismail, A. F., Aziz, F., Yusof, N., Bilad, M. R., Mohamud, R., Rahman, M. A. & Wan Salleh, W. N. 2022 A review of the potential of conventional and advanced membrane technology in the removal of pathogens from wastewater. *Separation and Purification Technology* **286**, 120454.

Nikpourian, H., Bahramian, A. R. & Abdollahi, M. 2020 On the thermal performance of a novel PCM nanocapsule: the effect of core/shell. *Renewable Energy* **151**, 322–331.

Ocakoglu, K., Dizge, N., Colak, S. G., Ozay, Y., Bilici, Z., Yalcin, M. S., Ozdemir, S. & Yatmaz, H. C. 2021 Polyethersulfone membranes modified with CZTS nanoparticles for protein and dye separation: improvement of antifouling and self-cleaning performance. *Colloids and Surfaces A: Physicochemical and Engineering Aspects* **616**, 126230.

Peng, H., Wang, J., Zhang, X., Ma, J., Shen, T., Li, S. & Dong, B. 2021 A review on synthesis, characterization and application of nanoencapsulated phase change materials for thermal energy storage systems. *Applied Thermal Engineering* **185**, 116326.

Qiu, Y., Ren, L. F., Shao, J., Xia, L. & Zhao, Y. 2022 An integrated separation technology for high fluoride-containing wastewater treatment: fluoride removal, membrane fouling behavior and control. *Journal of Cleaner Production* **349**, 131225.

Rodríguez-Cumplido, F., Pabón-Gelves, E. & Chejne-Jana, F. 2019 Recent developments in the synthesis of microencapsulated and nanoencapsulated phase change materials. *Journal of Energy Storage* **24**, 100821.

Roy, A., Venna, S. R., Rogers, G., Tang, L., Fitzgibbons, T. C., Liu, J., McCurry, H., Vickery, D. J., Flick, D. & Fish, B. 2021 Membranes for olefin–paraffin separation: an industrial perspective. *Proceedings of the National Academy of Sciences of the United States of America* **118** (37), e2022194118.

Saraç, E. G., Öner, E. & Kahraman, M. V. 2019 Microencapsulated organic coconut oil as a natural phase change material for thermo-regulating cellulosic fabrics. *Cellulose* **26** (16), 8939–8950.

Shchukina, E. M., Graham, M., Zheng, Z. & Shchukin, D. G. 2018 Nanoencapsulation of phase change materials for advanced thermal energy storage systems. *Chemical Society Reviews* **47** (11), 4156–4175.

Vadhera, J., Sura, A., Nandan, G. & Dwivedi, G. 2018 Study of phase change materials and its domestic application. *Materials Today: Proceedings* **5** (2), 3411–3417.

Vasu, A., Hagos, F. Y., Mamat, R., Kaur, J. & Noor, M. M. 2019 The effect of thermal cyclic variation on the thermophysical property degradation of paraffin as a phase changing energy storage material. *Applied Thermal Engineering* **149**, 22–33.

Wang, X., Shen, Y. & Lai, X. 2014 Micromorphology and mechanism of polyurethane/polyacrylate membranes modified with epoxide group. *Progress in Organic Coatings* **77** (1), 268–276.

Wang, Y. A., Smith, S. J. D., Liu, Y., Lu, P., Zhang, X., Ng, D. & Xie, Z. 2022 Surface hydrophilicity modification of thin-film composite membranes with metal – organic frameworks (MOFs) Ti-UiO-66 for simultaneous enhancement of anti-fouling property and desalination performance. *Separation and Purification Technology* **302**, 122001.

Xu, T., Fu, R. & Yan, L. 2003 A new insight into the adsorption of bovine serum albumin onto porous polyethylene membrane by zeta potential measurements, FTIR analyses, and AFM observations. *Journal of Colloid and Interface Science* **262** (2), 342–350.

Yang, L., Jin, X., Zhang, Y. & Du, K. 2021 Recent development on heat transfer and various applications of phase-change materials. *Journal of Cleaner Production* **287**, 124432.

Zhang, N. & Yuan, Y. 2020 Synthesis and thermal properties of nanoencapsulation of paraffin as phase change material for latent heat thermal energy storage. *Energy and Built Environment* **1** (4), 410–416.

Zhao, C., Xue, J., Ran, F. & Sun, S. 2013 Modification of polyethersulfone membranes – a review of methods. *Progress in Materials Science* **58** (1), 76–150.

Zhi, M., Fan, R., Yang, X., Zheng, L., Yue, S., Liu, Q. & He, Y. 2022 Recent research progress on phase change materials for thermal management of lithium-ion batteries. *Journal of Energy Storage* **45**, 103694.

First received 30 March 2023; accepted in revised form 11 August 2023. Available online 24 August 2023